Reactivity of succinic anhydride at lithium and graphite electrodes

Christopher Charton, J. Santos-Pena, Agnès Biller, Eric de Vito, Hervé Galiano, Matthieu Le Digabel, Daniel Lemordant

Reactivity of Succinic Anhydride at Lithium and Graphite Electrodes

Christopher Charton,[a,b] Jesùs Santos-Peña,[b,c] Agnès Biller,[a,b] Eric De Vito,[d] Hervé Galiano,[b,e] Matthieu Le Digabel,[a,b] and Daniel Lemordant[b,c,*,z]

[a]*CEA/DAM, Le Ripault, 37260 Monts, France*
[b]*Laboratoire de Recherche Correspondant, LRC CEA/PCM2E, France*
[c]*Université François Rabelais de Tours, Faculté des Sciences et Techniques, PCM2E, 37200 Tours, France*
[d]*CEA de Grenoble, LITEN, 38043 Grenoble Cedex 9, France*
[e]*CEA/DAM, Île-de-France, 91327 Bruyères-le-Châtel, France*

Succinic anhydride (SA) is an useful electrolyte additive for high voltage cathodes but has also a negative impact on graphite (Gr) or Li anodes. For this reason, the Li/electrolyte and Gr/electrolyte interfaces were investigated at 20°C and 45°C using half or symmetrical cells. When SA is added at 1% by weight to the electrolyte (alkylcarbonate mixture + $LiPF_6$), an increase in the Li/Li cell impedance at 20°C occurs owing to the formation of a resistive solid electrolyte interphase (SEI), composed of an inorganic inner layer and an organic outer layer, whereas at 45°C or in absence of SA, the interphase is more inorganic in nature. The reversible capacity of graphite, cycled in Gr/Li half-cells in the presence of SA, is very low at 20°C but almost ten times larger at 45°C. Cycling symmetrical Gr/Gr cells at 45°C indicates that Gr capacity is lower in the presence of SA in connection with the presence of an organic and polymer rich SEI. GC-MS analysis of the electrolyte after cycling shows that ethylene glycol bis-(alkylcarbonate) derivatives disappear when SA is present, owing to the ability of SA to react with lithium alkoxides to yield oligopolyester.
 [DOI: 10.1149/2.0621707jes]

Manuscript submitted February 20, 2017; revised manuscript received April 21, 2017. Published May 11, 2017.

Lithium ion batteries (LIBs) are a reliable way to store electric energy, with high gravimetric and volumetric energy density, which allows their application in nomad systems including electric and/or hybrid vehicles. However, electric vehicles range is unsuitable for most of the consumers and, therefore, energy density should be improved. In the past twenty years, many researches have been performed on electrode materials and electrolytes with the aim to enhance battery performance. Use of 5V class positive electrodes (cathodes) is a convenient way to increase LIBs energy density. It explains the development of promising "high voltage" materials like $Li_3V_2(PO_4)_3$,[1] Li_2CoPO_4F[2] or the $LiNi_{0.5}Mn_{1.5}O_4$ (LNMO)[3] spinel.

Nevertheless, the use of new cathodes operating at high voltage leads to the degradation of the battery electrolyte, usually based on a mixture of cyclic and linear alkylcarbonates containing $LiPF_6$ as salt and functional additives. Unfortunately, standard electrolytes are oxidized on 5 V cathodes and this significantly limits the battery cycling life. From the first cycles, electrolyte components degrade forming by-products, which in turn, can interact with electrodes surface. As an example, a passive layer is formed on graphite (Gr)/electrolyte interface at the first charge. This layer, known as the Solid Electrolyte Interphase (SEI), has a strong impact on the LIBs performances. Electrolyte formulation influences the chemical nature and structure of the SEI. With the aim to improve SEI quality and stability, SEI-forming additives like vinylene carbonate (VC) are generally added to the electrolyte in low amount (less than 5% by weight). These additives are designed to generate a protective passive layer on the active material surface preventing continuous electrolyte decomposition reactions.

Whereas additives can be a suitable option for enhancing battery performances, their use for protecting cathodes is less common, due to the inherent instability of the surface film formed on the positive electrodes against dissolution, chemical or electrochemical transformation.[4] Nevertheless anhydrides additives like succinic anhydride (SA) have a beneficial effect on Gr/LNMO cells,[5] enhancing capacity retention, battery cycling and coulombic efficiency with a marked reduction of the self-discharge due to the creation of a thin protective layer on the positive electrode. As pointed out by V. Tarnopolskiy et al.,[6] among many additives tested, only SA is efficient for using LMNO as a positive electrode and is able to reduce significantly the self-discharge of the electrode. In the same work, SA concentration in the electrolyte has been varied from 1% to 8% by weight, but only a slight influence was found on the performances of the Gr/LNMO cell. In order not to alter the main physicochemical characteristics of the electrolyte and prevent possible interferences with the anode, the lowest amount (1%) of additive maintaining the cell performances was selected for the present study. This feature reveals the importance of understanding the formation of passive layers to apprehend and optimize LIBs performances.

Half-cells, using lithium as counter electrode, are not well designed for studying electrode/electrolyte interfaces owing to possible parasitic reactions on metallic lithium generating by-products able to migrate and react on the opposite interface. In order to avoid these parasitic reactions, an ingenious system composed of two identical electrodes was introduced by Chen et al. in 2001.[7] This symmetrical system was originally designed to understand the impedance rise in LiB during storage.[7] Since the first introduction of symmetric cells, many studies have been performed to investigate the effect of additives like VC, vinyl ethylene carbonate (VEC), trimethoxyboroxine (TMOBX), lithium bis-(trifluoromethanesulfonyl) imide (LiTFSI) and fluoroethylene carbonate (FEC).[8] Those studies contribute to highlight the fact that some additives could act as well at the positive and the negative electrodes. Symmetric cells were also used to investigate electrode interfaces and electrolyte degradations[9] by combining electrochemical impedance analysis (EIS) and gas-chromatography mass spectra analysis (GC-MS) on post-mortem cells. LNMO/LNMO symmetric cells were also used by Demeaux et al. to study the degradation of the LNMO interface which was mainly attributed to manganese and nickel dissolution.[3] Hence, using symmetric cells is a convenient method for studying electrodes interfaces. In the current work, Li/Li and Gr/Gr cells have been built and cycled in a standard electrolyte containing or not SA as SEI additive. Changes in the lithium/electrolyte or graphite/electrolyte interfaces during cycling were followed by electrochemical impedance spectroscopy (EIS) and for Gr by X-ray photoelectron spectroscopy (XPS).[10] Complementary analyses of the electrolyte composition after cycling were performed by GC-MS experiments in order to assess electrolyte degradation mechanisms.

*Electrochemical Society Member.
[z]E-mail: daniel.lemordant@univ-tours.fr

Experimental

Materials.—Graphite electrodes, purchased from Hohsen Corp., are composed of 79 wt % of Gr (active material), 14 wt % of carbon black (conductive material) and 7 wt % of polyvinylidene difluoride (PVDF), as binder, casted on Cu foil (10 μm thick) current collector. Graphite loading is 5.1 mg.cm^{-2} and typically 50 microns thick.

Electrolyte preparation, 2032-type coin cells assembly and preparations for GC-MS analysis were all performed in argon-filled glove box ([H_2O] < 0.5 ppm and [O_2] < 20 ppm) at room temperature. Electrolytic solutions EMC-$LiPF_6$ (1 M), EC/EMC (1:1 w/w)-$LiPF_6$ (1 M) and EC/EMC (1:1 w/w)-$LiPF_6$ (1 M) + 1% SA were prepared with EMC and EC purchased from Novolyte Technologies (purity ≥ 99.9%). Succinic anhydride (purity = 99.9%) and $LiPF_6$ (Battery grade) were furnished by Across Organics and Fluorochem, respectively. Prior to their use, all solvents were dried with a moisture trap (ChemGenes Corp.) Lithium foil (0.75 mm thick) used as counter and/or reference electrode was purchased from Alfa Aesar.

Electrochemical tests.—Li/Li cells were assembled with 2 lithium electrodes (Ø 16 mm) separated by a Viledon felt (Freudenberg, Ø 16.5 mm) and a Celgard 2400 separator (Ø 16.5 mm) in 2032-type coin cells. Evolution of the interfacial resistance was evaluated by means of EIS operating in the range of 100 kHz to 2.5 mHz with an amplitude of 5 mV. EIS measurements were conducted at the beginning and every 25 hours for a total time of 3 days.

2032-type Li/Gr half cells were assembled using a Gr electrode (Ø 16 mm) and a lithium counter electrode (Ø 16 mm) separated by a Viledon felt (Freudenberg, Ø 16.5 mm) close to Gr and a Celgard 2400 separator (Ø 16.5 mm) close to lithium. Three electrodes cells, purchased from Hohsen Corp. (HS-3E test cell), have a circular reference slot in which the lithium reference is inserted (16.15 mm < Ø < 24 mm).

Symmetric Gr/Gr cells were built using two Gr electrodes lithiated up to the half theoretical capacity (0.5 mole of lithium per 6 mole of carbon) under a C/10 rate. As prepared Gr electrodes have a potential close to 0.1 V vs. Li/Li^+. By this approach, the Gr/electrolyte interfaces are identical for both electrodes and the SEI is identical in composition and thickness. Half-lithiated Gr electrodes are removed from the cells, without washing. In order to measure the potential of each graphite electrode during the electrochemical tests, a three electrodes cell was built with $(Li_{0.5}C_6)_1$ (as working electrode), $(Li_{0.5}C_6)_2$ (as counter electrode) and metallic lithium as reference. Viledon (Ø 24 mm) and Celgard 2400 (Ø 24 mm) separators were placed between the working and reference electrodes. After building the cell with $(Li_{0.5}C_6)_1$ and $(Li_{0.5}C_6)_2$, the first full charge can be described as:

$$(Li_{0.5}C_6)_1 + (Li_{0.5}C_6)_2 \rightarrow 6(C)_1 + (LiC_6)_2 \quad [1]$$

Symmetric cells are cycled under a C/5 regime up to thirty cycles. With this cell configuration, dynamics study of interfaces can be achieved without having to use a lithium counter electrode. In order to form a reproducible SEI, the same electrolyte is used for preparing the half-lithiated Gr electrodes and cycling symmetric cells built with them.

Galvanostatic cycling and electrochemical impedance spectroscopy (EIS) measurements were performed with a VMP3 multichannel potentiostat (Bio-Logic Science Instruments). EIS plots were fitted with the software Zview from Scribner.

Gas chromatography–Mass spectra analysis.—In order to study by-products due to electrolyte degradation during cycling, cells were opened and the Viledon separator was removed and soaked in acetonitrile (Alfa Aesar, purity > 99.8%) for 24 hours (1.0 mL for a Ø 16.5 mm separator and 2.1 mL for a Ø 24 mm separator). Gas chromatography (GC) analyses were performed with a 7890A GC System and a HP5MS column (30 m × 250 μm × 0.25 μm) from Agilent Technologies. A constant sample volume of 1 μL was injected into the split/splitless injector at 180°C. GC was connected to a 5975C inert MSD mass spectrometer with a triple axis detector from Agilent Technologies. Perfluorotributylamine (PFTBA) fragments were used for calibrating the mass spectrometer. Molar masses were scanned from 15 to 300 uma. Compounds and mass spectra identifications were realized according to the National Institutes of Standards and Technology (NIST) library.

Post-mortem analyses of electrodes.—Prior to surface analysis by X-rays photoemission spectroscopy (XPS) or FT-IR, electrodes were removed from the de-assembled cell and vacuum dried overnight.

FT-IR analysis.—FT-IR analyses were conducted on a Spectrum II spectrometer from PerkinElmer placed in a glove box. An ATR module with a germanium crystal was used to record infrared spectra from 400 to 4000 cm^{-1} at room temperature with an accuracy of 1 cm^{-1}.

XPS analysis.—After 24 hours drying under vacuum, electrodes samples were mounted on a sample holder with the help of double-sided copper adhesive tape. It was then transferred to a PHI VersaProbe II XPS spectrometer by using a sealed transfer vessel to avoid exposure to air. Standard conditions, involving an Al Kα monochromatic X-ray source (hν = 1486.7 eV) and a take-off angle of 45° from the surface, were used for all the XPS analyses. Spectra were recorded with a pass energy of 23.5 eV and an energy step of 0.1 eV. Profiles were obtained by sputtering a mono-atomic Ar ions beam (at 2 keV/2 μA) and rastered on a 2 mm × 2 mm area. Analyses were achieved on a 100 μm × 100 μm area located at the center of the sputtered area. Double-charge compensation (flood gun & ion gun) was used during the experiment to avoid charge effects. The vacuum recorded during the analyses was always below 5 10^{-9} mbar. Data were analyzed and spectra were fitted with the help of PHI Multipak software.

Results and Discussion

Reactivity of SA with lithium and lithiated graphite.—*Li/Li symmetric cells at OCV.*—Electrode/electrolyte interface has been studied by electrochemical impedance spectroscopy (EIS) using symmetrical Li/Li cells. In order to follow the modifications brought to the interfaces by the reaction between Li and the EMC ($LiPF_6$, 1 M) or EC/EMC ($LiPF_6$, 1 M) electrolytes, measurements were carried out just after the cell assembly and then every 25 hours. The imaginary and real part of the complex impedance were measured at 20°C and plotted as a Nyquist diagram in Fig. 1 for the EMC ($LiPF_6$, 1 M) and EC/EMC ($LiPF_6$, 1 M) electrolytes containing or not 1% of SA.

The impedance diagram exhibits a well-defined slightly depressed half-circle in the high-medium frequency range which reflects the interfacial impedance including SEI film and charge transfer resistances. In the low frequency range (below 1 Hz), an ill-defined curve is observed which cannot be clearly attributed to a diffusion process. In EMC electrolyte, little variations occur at the interface as the circle diameter and the frequency at the apex of the half-circle, related to the apparent time constant of the system (τ = RC) remains almost constant with time. This means that the SEI is formed rapidly and is stable. In the EC/EMC electrolyte, the lithium interphase is not as stable as the half-circle increases in diameter with time meaning that the SEI layer is growing upon contact between electrolyte and lithium. Nevertheless the frequency at the top of the half-circle in the EC/EMC electrolyte is not affected by the electrode/electrolyte exposure time. As a partial conclusion, the EC component of the blended electrolyte is more reactive toward lithium than EMC.

When SA is added to the EC/EMC electrolyte, the half-circle becomes almost ten times larger in diameter and expands very fast during the first 24 h of electrode exposure to the electrolyte. Moreover, the frequency at the apex of the half-circle shifts from 25 Hz at t = 0 to 8 Hz at t = 75h as pointed out on the graph reported in Fig. 1. This shift in frequency is linked to a variation in the time constant of the equivalent R//C circuit and indicates a corresponding increase in RC values. This point will be discussed in the following paragraph.

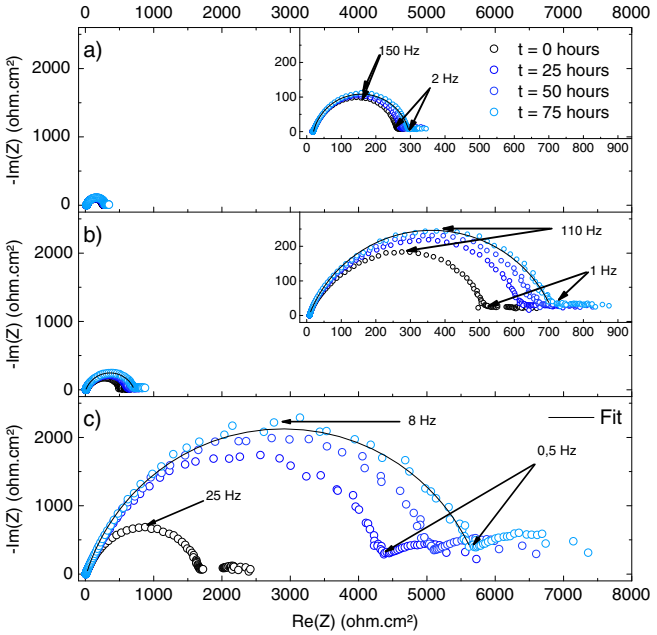

Figure 1. EIS measurements made at 20°C every 25 hours on Li/Li symmetric cells containing: (a) EMC ($LiPF_6$, 1 M), (b) EC/EMC ($LiPF_6$, 1 M) without SA and (c) with 1% of SA.

As proposed by Thevenin and Muller,[11] it is possible to simulate the impedance results by the simple equivalent electrical circuit shown in Fig. 2. Within this scheme, are placed in series the electrolyte bulk resistance (R_e) and a R//C parallel element representing the apparent interfacial resistance R_i (SEI and charge transfer contributions) coupled to the apparent interfacial capacitance C_i (SEI charge storage and double layer contribution). Half-circle in Fig. 1 are slightly depressed so the capacitance element C_i must be replaced by a constant phase element (CPE). CPE characteristics are Q_i, the pseudo-capacitance, and $\phi = -90.\alpha$, the corresponding phase angle in the Nyquist plot. The pseudo-capacitance Q_i can be converted into true capacitance value C_i by using Equation 1:[12]

$$C_i = {Q_i}^{1/\alpha} {R_i}^{(1-\alpha)/\alpha} \quad [2]$$

where R_i is the resistance in parallel with the CPE in the equivalent circuit.

A low frequency tail on the Nyquist plot is usually seen when lithium is in contact with alkylcarbonate solvents[11,13] or even polymer membranes (Li-PEO-LiTFSI/Li system).[14] Lewandowski et al. have fitted the low frequency tail by an element Z without any physical meaning as it cannot correspond to a Warburg element. This phenomenon remains unknown and, in consequence, it appears useless to fit all of the impedance spectrum but the half half-circle.

The electrolyte resistance R_e remains almost constant with time: $R_e = 18.9$, 8.2 and 8.0 Ω cm^2 for respectively the EMC and EC/EMC electrolytes without and with SA additive. However, the most pertinent parameters for understanding the formation and evolution of the lithium/electrolyte interface remain R_i and C_i and, complementarily

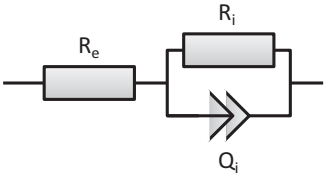

Figure 2. equivalent circuit used to fit EIS measurements on Li/Li symmetrical cell.

their product, which is equal to the time constant τ ($\tau = R_iC_i$) of the RC circuit. Variations of the three parameters with time are displayed in Fig. 3.

According to Thevenin and Muller,[11] a constant value of τ indicates that the SEI model based on a film rich in inorganic compounds applies well and this is the case for the electrolytes without additive. Nevertheless, in the presence of SA even at a low concentration (1%), τ increases with time and hence it is not possible to attribute the half-circle to a simple conduction process in a solid electrolyte according to the SEI model. The apparent capacitance decreases slightly with time but is 50% higher in the electrolyte containing SA.

A compact-stratified layer (CSL) model which is composed of two sub-layers should be more adequate to describe the interface. One of such layers is the solid electrolyte interphase (rich in mineral compounds) and the other a solid or porous organic polymer layer. Fitting the results by an equivalent electrical scheme is complex and well beyond the scope of this work.

In order to confirm this different nature of the SEI depending on the presence or the absence of SA and in the framework of the SEI model for a planar system of unit area, it is convenient to link Ri, Ci values to the thickness (x), of the surface film and to its intrinsic conductivity (σ) and permittivity (ε) as:

$$R_i = x/\sigma \quad [3]$$

$$C_i = \varepsilon/x \quad [4]$$

Using relation 1 and 2, the time constant τ can be defined as:

$$t = R_iC_i = \varepsilon/\sigma \quad [5]$$

Hence, τ will only depend on intrinsic characteristics of the SEI and will remain constant if the interphase is homogeneous in structure and composition. For the EMC and EC/EMC electrolytes the time constants are respectively 3.63 and 5.85 ms after 24h of storage, indicating a stable SEI.

Taking a mean value for the relative permittivity $\varepsilon_r = 10$ for the SEI layer, the conductivity σ can be roughly estimated to be respectively 2.45 10^{-10} S cm^{-1} and 1.51 10^{-10} S cm^{-1} for EMC and EC/EMC electrolytes, respectively. This is a suitable range of magnitude[11] if we take into account the electrical properties of solid electrolytes like Li_2CO_3 and Li_2O for which the conductivity is in the range of 10^{-10} S cm$^{-1} < \sigma < 10^{-8}$ S cm^{-1}. Therefore, the SEI model applies quite well for those electrolytes. At the opposite and following the CSL model, the presence of a polymeric phase (like polypropylene oxide $(PPO)_x$) in the outer part of the interphase, for which the conductivity is at least one order of magnitude larger, will not explain satisfactorily the observed time constants. It is highly probable that when SA is added to the electrolyte, a polymeric phase will be present and this will be confirmed thereafter. Valuable information concerning this point is also provided by measurements at higher temperatures as presented below.

Effect of the temperature.—The impact of raising the temperature from 20°C to 45°C on the apparent interfacial resistance R_i is shown in Fig. 4 for both studied electrolytes. A linear dependence of R_i with the time square root indicates that the SEI growth is controlled by diffusion of electrolyte components. A change in the SEI structure or depletion of SA after 25 h of contact with the electrolyte accounts for the slope break, suggesting that the new structure has a slower growth or a lower conductivity.

A beneficial effect of rising the temperature to 45°C is the decrease of the interfacial resistance $R_i \approx R_{SEI}$. After 100 hours of storage, R_i value decreases from 6000 Ω cm^2 at 20°C to 1000 Ω cm^2 at 45°C, a value which is similar to that obtained without SA. This decrease cannot only be interpreted on the basis of an increased ionic conductivity of the mineral layer (according to the CSL model) but rather on a structure change of the outer layer of the interphase. It is very likely that the outer layer which is mainly polymeric undergoes a change

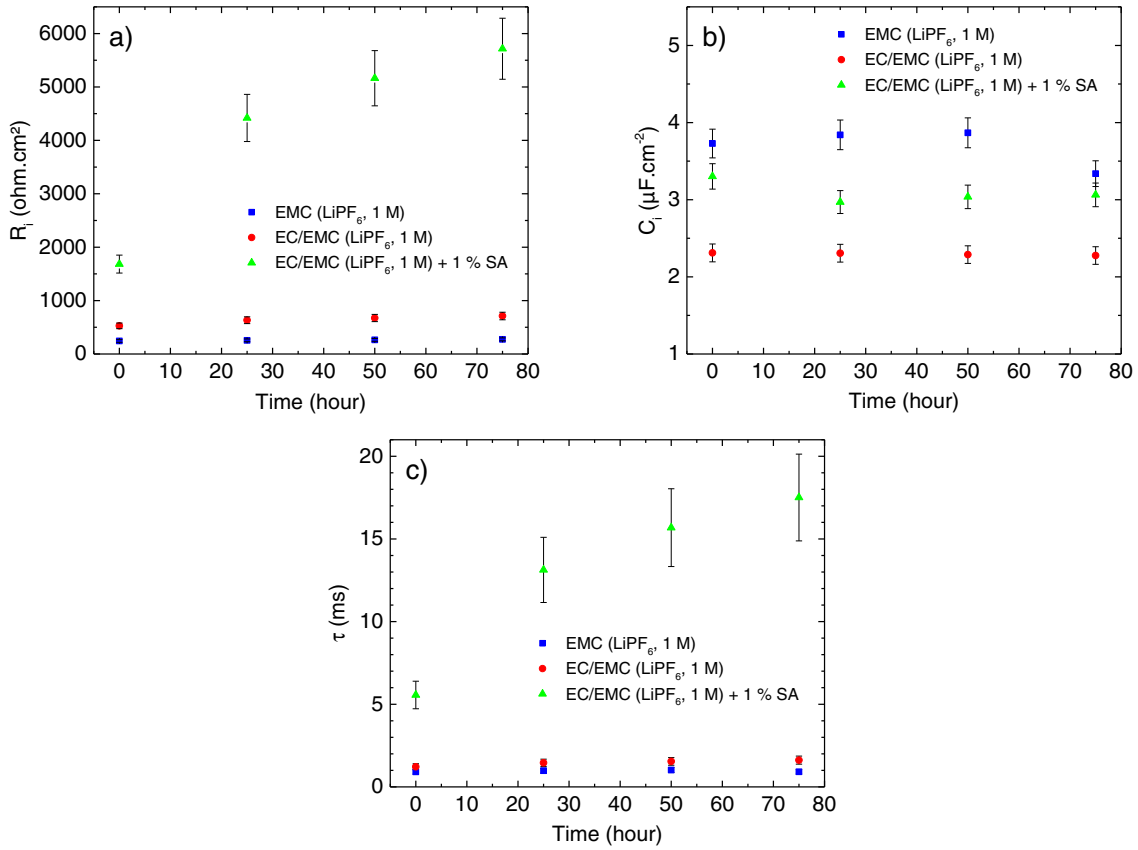

Figure 3. Plot of the apparent resistance, apparent capacitance and time constant for the equivalent circuit display in Fig. 2 vs. time for the first 75 hours of lithium in contact with the electrolytes.

in porosity or, in amorphous regions, a glass transition phenomenon. This hypothesis will be supported thereafter by experimental results.

As a partial conclusion, the reactivity between metallic lithium and electrolytes with or without SA additive have been be evaluated by EIS measurements using Li/Li symmetric cells. The addition of 1% of SA has a strong impact on the reactivity of EC/EMC ($LiPF_6$, 1 M) toward metallic lithium leading to a stratified SEI which is globally more organic in composition according to the CSL model and very sensitive to temperature variations.

This study will be now focused on reaction and degradation mechanisms at the Graphite/electrolyte interface in the presence of SA additive. Metallic lithium will not be used as counter electrode due to its instability against this additive and the temporal evolution of the interfacial layer.

Li/Gr half-cells after one cycle at 20°C and 45°C.—Fig. 5 shows the first galvanostatic charge/discharge cycles at 20°C and 45°C of Li/Graphite half-cells with an electrolyte containing EC/EMC ($LiPF_6$, 1 M) with 1% SA. The theoretical capacity of graphite is 372 mA h g^{-1}, but the capacity provided by graphite in these experiments is only 50 mA h g^{-1} at 20°C and 265 mA h g^{-1} at 45°C. In agreement with previous results obtained with Li/Li cells, this means that lithium ion insertion in graphite is blocked at 20°C when the electrolyte contains

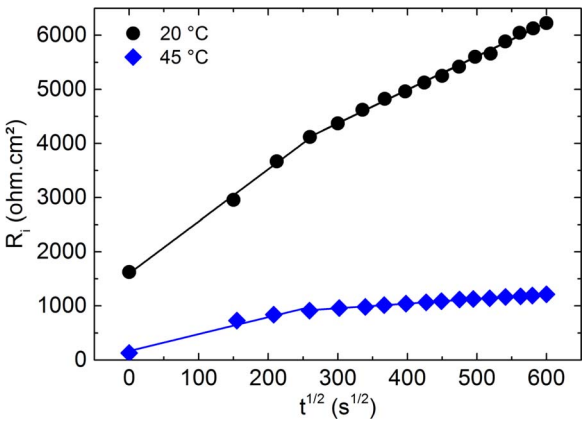

Figure 4. $R_i = f(t^{1/2})$ for Li/Li symmetric cells containing EC/EMC ($LiPF_6$, 1 M) +1% of SA at 20°C and 45°C.

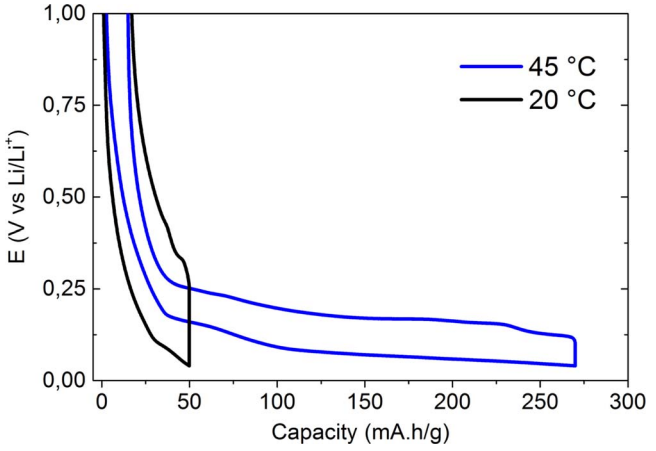

Figure 5. Galvanostatic first cycles at C/10 rate and two temperatures (20°C and 45°C) of Li/Gr half-cells containing EC/EMC (LiPF6, 1 M) and 1% SA.

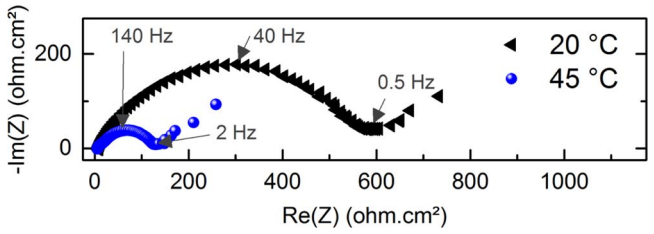

Figure 6. EIS measurements at the lithiated state performed after 1 cycle (C/5, D/5) at 20°C and 45°C on Li/Gr half cells containing EC/EMC (LiPF6, 1 M) with 1% of SA.

1% of SA. To confirm this point, we have performed two electrodes EIS measurements at the lithiated state on Li/Gr half-cells after one cycle. Nyquist diagrams, collected at 20°C and 45°C are displayed in Fig. 6.

Despite the fact that in this configuration (Li/Gr cell) EIS contains the response of both the graphite/electrolyte and the lithium/electrolyte interfaces, it is nevertheless clear that the cell impedance drastically decreases when the temperature is raised to 45°C. It is a matter of fact that the graphite SEI becomes less resistive to lithium ions migration through its structure as proved by the profile of the galvanostatic charge reported in Fig. 5. Nevertheless, in order to clarify this point, symmetric Gr/Gr cells have been built and studied in the following.

To sum up, the poor specific capacity provided by the graphite electrode at 20°C in Li/Gr cells indicates that the SA has a negative impact on the graphite SEI.

Reactivity of SA toward lithiated graphite in symmetric cells.— *Electrochemical tests.—Galvanostatic cycling of Gr/Gr cells.*—Pre-lithiation of graphite and cycling tests have been conducted in Li/Gr half-cells at 45°C. For pre-lithiation, the graphite electrode was charged in lithium up to a composition of $Li_{0.5}C_6$ (half the theoretical capacity of Gr) in a cell containing the reference electrolyte with or without SA. When a symmetric cell is assembled, both electrodes are at a potential close to 100 mV vs. $Li/Li^+$and consequently, the full cell voltage is nearly zero. During the full cell charge, and according reaction 1, one electrode is lithiated while the other is delithiated. During the discharge, the inverse reactions take place but the difficulty in charge balancing of both electrodes impacts the cycling results. A lithium reference electrode has been introduced to determine the potential of each electrode. In this configuration, the potential of graphite electrodes has been let to vary between 20 mV and 2 V vs. Li/Li^+ and hence, the full cell voltage oscillated between −2 V and 2 V. For instance, the cycling behavior at C/5 rate of a symmetric Gr/Gr cell containing EC/EMC ($LiPF_6$, 1 M) at 45°C is displayed in Fig. 7. Blue and red curves correspond to the potential of each Gr electrode vs. the lithium reference electrode and the black curve is the voltage of the full symmetric cell. Evolution with cycle number of symmetric Gr/Gr cells capacity at 45°C in the electrolytes containing or not SA is plotted in Fig. 8.

The impact of SA added to the electrolyte is depicted by the graphs reported in Fig. 7. The cell cycled in the SA free electrolyte provides a reversible capacity at the first cycle of 315 mAh g^{-1} versus 265 mAh g^{-1} for the electrolyte with SA. During cycling, there is a trend for both cells capacity cells to fade. Thus, capacities at the 30th cycle are only 215 mAh g^{-1} and 142 mAh g^{-1}, respectively, without and with SA. The origin of the capacity fade during cycling, observed for both symmetric cells, is not clear and we can only assign it to the inadequate balancing of the Gr electrodes which play alternatively the role of cathode and anode.

As a conclusion, these results confirm once again the negative impact of SA on the graphite SEI. This additive decreases the reversible capacity of Gr upon cycling and, as an attempt to explain this phenomenon, it is expected that SA which is already known as a curing agent in polymer science,[15] may react at the Gr electrode and modify

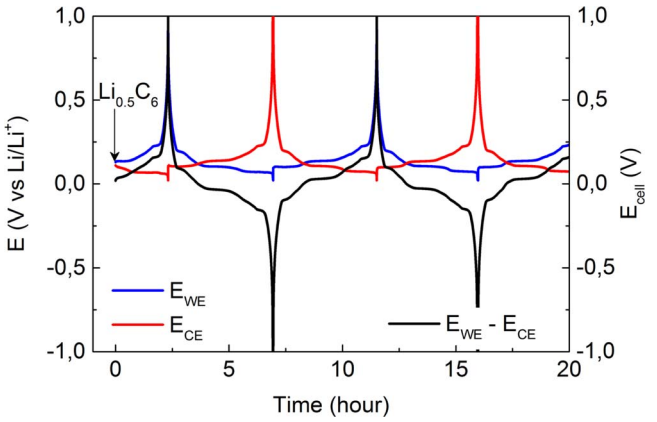

Figure 7. Cycling behavior of a 3 electrode symmetric Gr/Gr cell containing EC/EMC ($LiPF_6$, 1 M) at 45°C (C/5, D/5). Blue (—) and red curves (—) show the potential of each Gr electrode vs. Li/Li^+ reference electrode. The black curve (—) is the potential of the symmetric cell (V) during cycling.

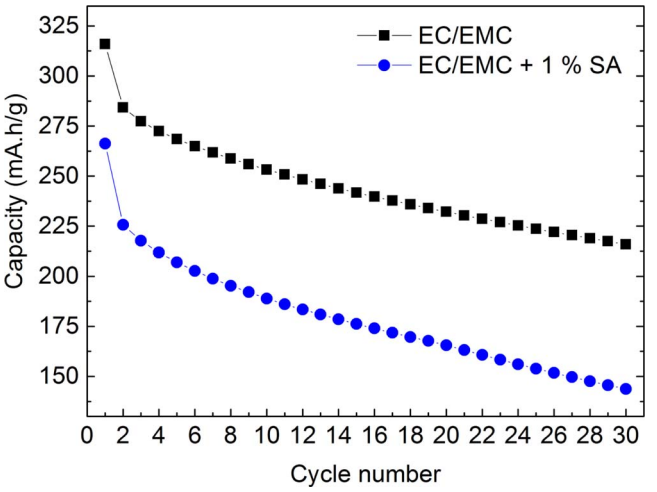

Figure 8. Cell capacity against cycle number for symmetric Gr/Gr cells containing EC/EMC ($LiPF_6$, 1 M) without and with 1% of SA (C/5, D/5, 45°C, 30 cycles).

the SEI composition (more organics). This will be validated in the next sections.

Electrochemical impedance spectra of Gr/Gr cells.—In order to deeper investigate SA influence on the graphite/electrolyte interfaces in symmetric cells, EIS measurements have been realized using a three electrodes configuration. Nyquist diagrams for the lithiated electrode (E≈ 50 mV vs. Li/Li^+) are shown in Fig. 9, after performing 30 cycles (C/5 rate) at 45°C. In order to fit experimental data, a modified Randles equivalent circuit as described in Fig. 10 has been employed.

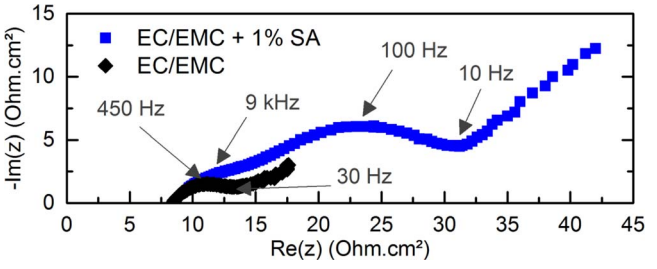

Figure 9. Nyquist diagram of lithiated Gr in symmetric Gr/Gr cell containing EC/EMC (LiPF6, 1 M) without and with 1% of SA after 30 cycles (C/5, D/5, 45°C).

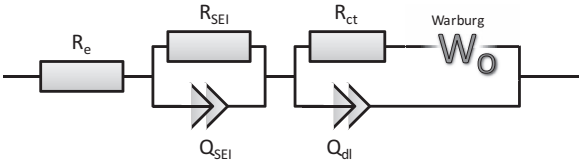

Figure 10. equivalent circuit used to fit the EIS results obtained with the Gr/Gr cells.

In this circuit, the electrolyte resistance (R_e) is placed in series with two R//C elements. The first one (R_{sei}/C_{sei}) corresponds to the SEI contribution and the second to the double layer capacitance (C_{dl}) in parallel with the charge transfer resistance (R_{ct}) and a Warburg (Wo) element. In the electrolyte free of SA, the SEI provides a half-circle which is difficult to identify but necessary for fitting data. When SA is present the half-circle is clearly visible. Fitting EIS measurements by the equivalent electrical scheme displayed in Fig. 10, are reported in Table I.

The main feature is a large increase in SEI and charge transfer resistances in the presence of SA. At the opposite the capacitance values are slightly or not modified. The increase in R_{sei} value means that either the film conductivity decreases in the presence of SA, either its thickness increases. Nevertheless, as the SEI capacitance is the same with or without SA, this indicates that the ratio ε/x remains also constant. Hence it is likely that the increase in R_{sei} is due to a decrease in conductivity owing to the presence of compounds formed by SA side-reactions and this will be confirmed by the XPS study. Finally, the charge transfer resistance is also higher in the presence of SA, which is commonly associated with the decrease ability of lithium ions to desolvate, cross the interface and insert between graphene planes. The next section will be devoted to investigate the SEI chemical nature by complementary techniques.

XPS analysis of lithiated graphite interfaces.—Symmetric Gr/Gr cells containing the EC/EMC electrolyte with or without SA were dissembled in a glove box after 30 cycles. Lithiated Gr electrodes were recovered and analyzed by X-Ray photoelectron spectroscopy (XPS) to study the chemical composition of the outer surface. In Fig. 11 is displayed as a bar graph, the atomic percentages for C, O, Li, F and P elements obtained by XPS. Detailed analysis of C 1s and O 1s core spectra is displayed in Fig. 12 after de-convoluting the peaks and chemical environment data for each element are collected in Table II. It is worth noting that Li 1s, P 2p and F 1s spectra (not shown here) were only slightly different regarding the presence of the SA.

Atomic percentages reported as a bar graph in Fig. 11 show that when SA is added to the electrolyte, there is a strong decrease in lithiated species (from 47.3% to 34.9%) and in agreement with this finding, the relative amount of fluorine is also reduced (from 31.2% to 26.0%). This feature is relevant for lithium species as Li_2CO_3 and especially LiF which ensure lithium ion transport through the SEI via Li_nF_m clusters. The stability of these clusters has been already demonstrated by DFT calculations[16,17] and studied by TOF-SIMS experiments.[18] They are able to provide conductivity to the SEI by a ion (Li^+ and F^-) hopping mechanism from cluster to cluster.

At the opposite, there is a larger amount of carbon and oxygen containing species in the sample which has been cycled in the presence of SA. This means that the reaction of SA at the graphite surface

Table I. fitting data to the equivalent circuit displayed in Fig. 10 for Gr/Gr cells. Values in brackets represent the standard deviation.

Electrolyte	R_e Ω cm^2	R_{SEI} Ω cm^2	C_{SEI} μF cm^{-2}	R_{ct} Ω cm^2	C_{dl} μF cm^{-2}
EC/EMC	8.4 (0.28)	0.2 (0.03)	28 (1.25)	2.7 (0.21)	41 (1.87)
EC/EMC + SA	9.0 (0.25)	5.4 (0.30)	2.5 (0.14)	16 (1.40)	60 (2.12)

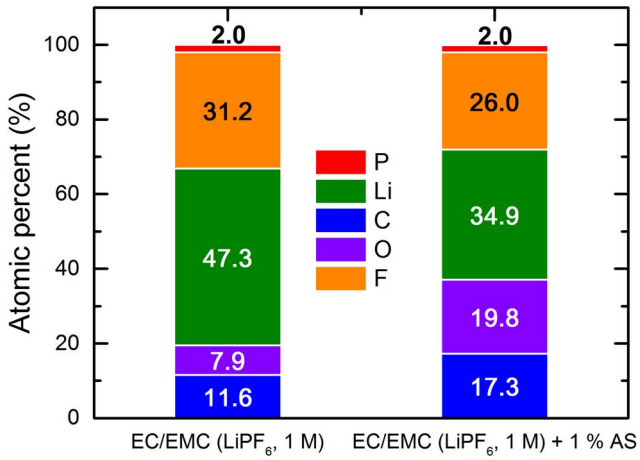

Figure 11. Elemental analysis of the SEI surface by XPS with or without SA added to the electrolyte

increases the amount of organics (semi-carbonates, alkoxides, ethylene glycol derivatives, etc.) and polymeric (PEO type) compounds that participate in the interphase composition. The atomic percentage in phosphorous compounds remains stable. Hence, the effect of SA on the SEI composition is similar to that observed on metallic lithium: the surface layer becomes richer in organic species at the expense of the mineral contribution, especially lithiated compounds.

A more detailed picture of the SEI composition is given by the results reported in Table II. Li 1s spectrum shows minor compounds like lithium oxide (Li_2O)[19] at the interface, organic (R-OCO_2Li) and mineral (Li_2CO_3) carbonates.[20] The most important feature in the Li 1s spectrum is a very high content in LiF[19,20] in the electrode cycled without SA. Nevertheless, when SA is added, the SEI becomes poorer in LiF as indicated by the decrease of Li 1s and F 1s signals and therefore lithium organic (R-OCO_2Li) and mineral (Li_2CO_3) compounds are present as minor species.

C 1s spectrum contains the signature of C-C and C-H bonds (284.8 eV),[21] C-O and O-C=O bonds (286.2 eV)[21] and O-C(O)=O carbonate groups (289.0 eV).[22,23] Most of these peaks can be assigned to organic compounds like poly(ethylene) oxide (PEO), lithium alkoxide (ROLi), lithium alkyl carbonates ($ROCO_2Li$)[24] and more complex compounds like ethylene glycol bis-(alkylcarbonate) (R-OOCO-CH_2CH_2-OCOO-R) at the electrode surface.[10] O 1s spectrum exhibits two main peaks at 531.7 (C-O) and 533.0 eV (O-C=O and O-C(O)=O) bonds in agreement with that found for the C 1s spectrum.[24] Finally, on the P 2p spectrum, Li_xPF_y and $Li_xPO_yF_z$ compounds are detected[20] at the Gr SEI surface in low amounts, their atomic percentage being limited to 2% with or without SA.

This XPS study confirms that SA induces a change in the SEI composition which becomes richer in organic compounds and poorer in mineral compounds referred to the electrodes of symmetrical cells tested in the electrolyte without SA.

Electrolyte analysis by GC-MS after cycling in Gr/Gr cells.—Electrolyte degradation occurs at the Gr interface when the SEI is formed or even during cycling if it is not stabilized. The variation in composition of the electrolyte was studied by GC-MS after performing 30 cycles at 45°C in symmetric Gr/Gr cell. For this purpose, the separator was recovered from coin cells, put into contact with pure acetonitrile and the resulting solution was analyzed. GC-MS chromatograms, obtained for the pristine and cycled electrolyte and the corresponding peaks assignment are shown in Fig. 13 and Table III respectively.

On pristine EC/EMC ($LiPF_6$, 1 M) electrolyte chromatogram, the three most important peaks correspond to acetonitrile (t = 1.63 min), EMC (t = 3.10 min) and EC (t = 8.39 min). There is a little peak at t = 1.88 min which was identified as propionitrile, an impurity intrinsic to acetonitrile. At short times, there are two peaks which are

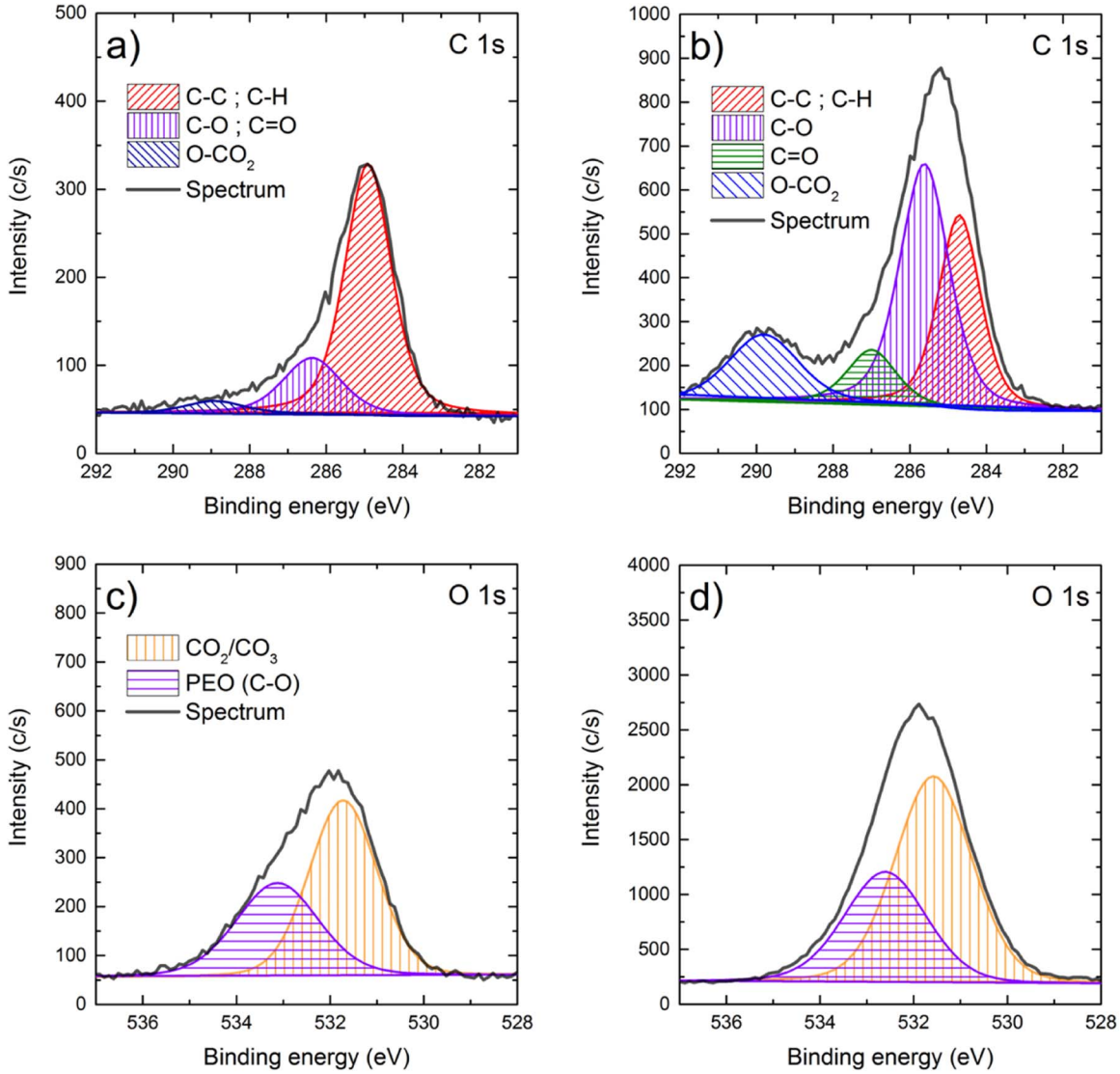

Figure 12. C 1s and O 1s spectra of lithiated Gr electrodes after 30 cycles at 45°C in Gr/Gr symmetric cells containing EC/EMC ($LiPF_6$, 1 M) without (a, c) or with 1% SA (b, d).

assigned to POF_3 (t = 1.28 min)[25] and PF_5 (t = 1.39 min).[26] These compounds come from the PF_6^- anion thermal degradation according to the following reaction:[27]

$$LiPF6 = LiF + PF_5 \rightarrow H_2OPOF_3 + 2HF \quad [6]$$

Table II. Atomic percentage report determined by XPS analysis of Gr surface after 30 cycles in symmetric Gr/Gr cell containing EC/EMC ($LiPF_6$, 1 M) electrolyte without and with SA.

	Species/bonds	EC/EMC ($LiPF_6$, 1 M)	EC/EMC ($LiPF_6$, 1 M) + 1% SA
Li 1s	Li_2O	1.9	1.6
	LiF Li_2CO_3 $ROCO_2Li$	45.4	33.3
C 1s	C-C C-H	8.6	6.1
	C-O O-C=O	2.6	8.5
	CO_3	0.4	2.7
O 1s	C-O	4.7	13.3
	CO_2 CO3	3.2	6.5
F 1s	Li_nF_m	28.2	22.4
	C-F Li_xPF_y	3.0	3.6
P 2p	Li_xPF_y	0.2	0.1
	$Li_xPO_yF_z$	1.8	1.9

The last two peaks correspond to dimethyl carbonate (2.11 min) and diethyl carbonate (4.57 min) which are also initially present in EMC solvent as impurities. When Gr/Gr cells are cycled in the electrolyte without SA, three new peaks located at 11.8 minutes, 12.9 minutes and 13.9 minutes arise which are assigned respectively to ethylene glycol bis-(methyl carbonate), ethylene glycol ethylmethyl bis-(carbonate), ethylene glycol bis-(ethyl carbonate).[28] These bis-(alkyl carbonates) are depicted (molar masses and chemical structure) in Table IV.

These compounds have been earlier identified as electrolyte degradation byproducts,[29] and form on the graphite electrode according to the reduction mechanism[30,31] reported in Fig. 13.

The chromatogram obtained with the electrolyte containing 1% of SA, is similar excepted for the new peak at 9.10 min which is assigned to SA and the disappearance of the peaks corresponding to the bis-(alkyl carbonates). This means that SA is still present in the electrolyte after 30 cycles. As mentioned above, SA is a good curing agent used in polymer chemistry[15] and hence, this reactive molecule is able to participate in numerous reactions occurring at the electrode

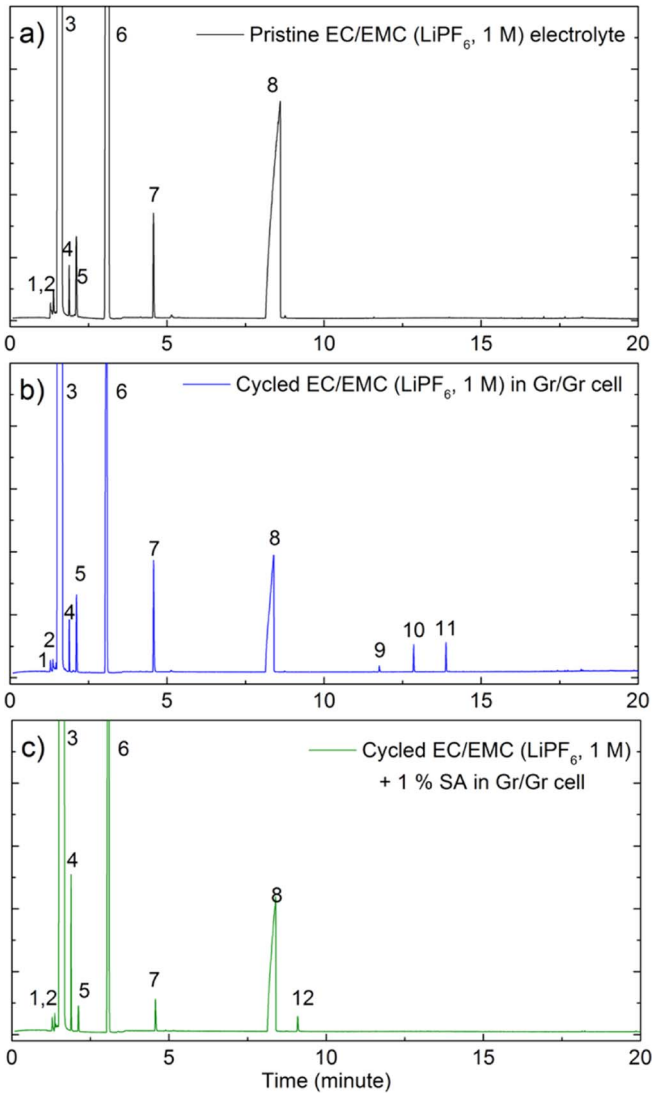

Figure 13. GC chromatogram of electrolytes: (a) pristine EC/EMC ($LiPF_6$, 1 M), (b) cycled EC/EMC ($LiPF_6$, 1 M) and (c) cycled EC/EMC ($LiPF_6$, 1 M) + 1% SA. Galvanostatic cycling was performed in Gr/Gr symmetric cell and electrolytes were collected after 30 cycles (C/5, D/5, 45°C).

Table III. Peaks assignment for the GC chromatograms displayed in Fig. 12.

Peak number	Time (min)	Molar mass ($g.mol^{-1}$)	Compound
1	1.28	104	POF3
2	1.39	126	PF_5
3	1.63	41	Acetonitrile (ACN)
4	1.88	55	Propionitrile (impurity present in acetonitrile)
5	2.11	90	Dimethyl carbonate (DMC)
6	3.10	104	Ethylmethyl carbonate (EMC)
7	4.57	118	Diethyl carbonate (DEC)
8	8.39	88	Ethylene carbonate (EC)
9	11.76	178	Ethylene glycol bis-(methyl carbonate) (EGBMC)
10	12.86	192	Ethylene glycol methylethyl bis-(carbonate)
11	13.88	206	Ethylene glycol bis-(ethyl carbonate) (EGBEC)
12	9.10	100	Succinic anhydride (AS)

Table IV. Ethylene glycol derivatives found in the used EC/EMC ($LiPF_6$, 1 M) electrolyte after 30 cycles in symmetric Gr/Gr cell at 45°C.

Ethylene glycol bis-(methyl carbonate) Time retention: 11.8 min M = 178.14 g/mol	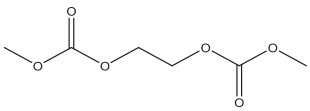
Ethylene glycol methylethyl bis-(carbonate) Time retention: 12.9 min M = 192.17 g/mol	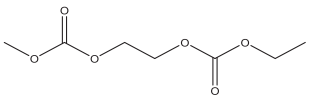
Ethylene glycol bis-(ethyl carbonate) Time retention: 13.9 min M = 206.19 g/mol	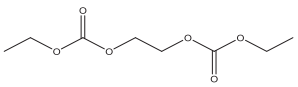

interface. Their products would probably modify the SEI composition, as observed by means of XPS analysis.

SA reaction at negative electrodes (Li, Gr) and validation by FTIR analysis.—As mentioned above, bis-(alkyl carbonates) are not present in the cycled electrolyte when it contains SA. In order to explain this feature, one must take into account that the SEI formed onto

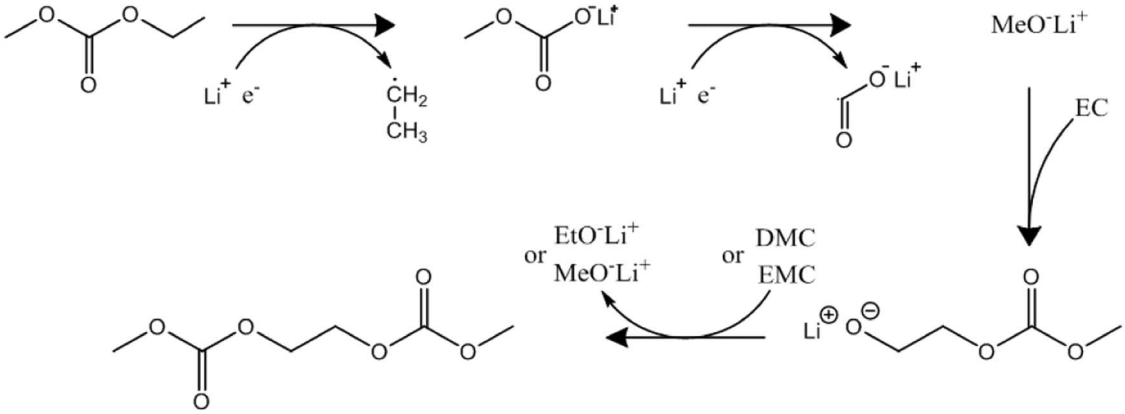

Figure 14. GC chromatogram of electrolytes: (a) pristine EC/EMC ($LiPF_6$, 1 M), (b) cycled EC/EMC ($LiPF_6$, 1 M) and (c) cycled EC/EMC ($LiPF_6$, 1 M) + 1% SA. Galvanostatic cycling was performed in Gr/Gr symmetric cell and electrolytes were collected after 30 cycles (C/5, D/5, 45°C).

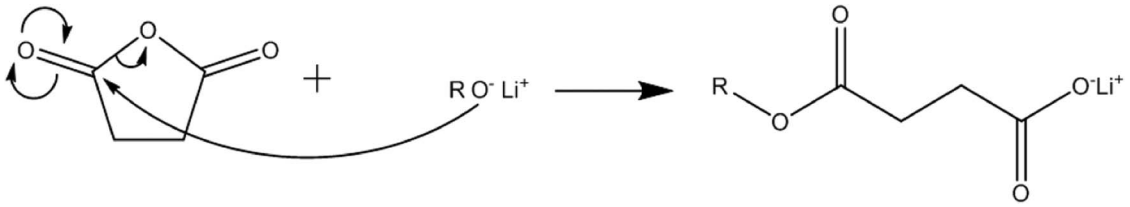

Figure 15. Ring opening of SA by lithium alkoxides.

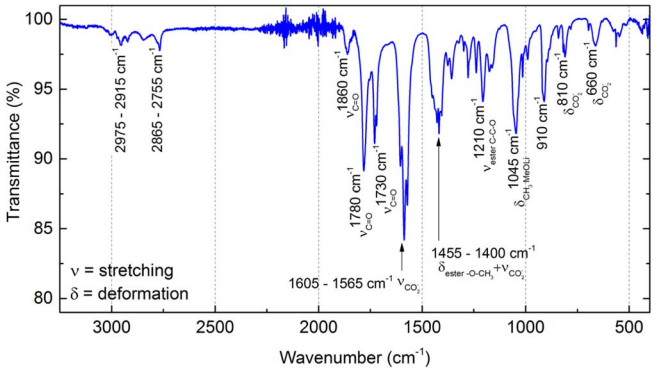

Figure 16. Infrared spectrum of the white solid deposit obtained by reaction of SA with lithium methoxide.

negative electrodes like Li or Gr always contains lithium alkoxides. These organic compounds can open the ring of 5 membered heterocyclic molecules like EC or PC and SA in a similar manner. A possible mechanism scheme for this reaction is displayed in Fig. 15.

According to such mechanism, the product of the reaction of SA with a lithium alkoxide is 4-alkoxy-4-butanoate. This compound may, subsequently, react with another SA molecule to form a more complex molecule like a polysuccinate ester or with an EC molecule to form a polysuccinate ester containing carbonate moieties. In order to check this hypothesis, a simple test was performed. In a vial, 6 mmol of SA were added to 5.2 mmol of lithium methoxide dissolved in 10 mL of DMC. Lithium methoxide/SA reaction kinetics is slow in presence of DMC. However, after 24 h, a white solid is deposited. The solution is filtered and the deposit dried under reduced pressure before performing FT-IR analysis. The spectrum of the solid deposit is displayed in Fig. 16. The assigned main vibrational bands together with their wavenumber are indicated on the spectrum.[33–39] Main peaks belong to the ester functional group (methyl ester especially) and lithium carboxylate groups ($ROCO_2^-Li^+$). Traces of lithium methoxide and SA reactants are also present.

Vibrational bands identified on the IR spectrum are in agreement with the structure of a polysuccinate ester and this allows validating the proposed reaction scheme. As this compound is not soluble in alkylcarbonates solvents, it is not surprising to find it as a component of the outer part of the SEI formed on Gr in the EC/EMC electrolyte. This finding contributes also to explain satisfactorily the richness in C and O SEI elements when SA is present and the deficiency in F and Li leading to a poorly ionic conductive SEI as indicated by EIS measurements. Increasing the temperature to 45°C will probably limit polymer formation and depositing on graphite. Additionally, it can also explain the slow-down of the SEI growth rate observed on lithium when the temperature is raised to 45°C on lithium.

Conclusions

The effect of succinic anhydride, dissolved in an EC/EMC-$LiPF_6$ electrolyte, on lithium and graphite electrode interfaces has been studied with the aim to determine the mechanisms implied. It has been first shown that the addition of 1% of SA to the electrolyte increases the impedance of the lithium/electrolyte interface drastically at 20°C. The SEI growth at the lithium/electrolyte interface is controlled by diffusion with a strong dependency on the temperature as at 45°C the SEI growth rate is slower. In the presence of SA in the electrolyte, the Gr reversible capacity is as low as 25 mA h g^{-1} at 20°C but ten times larger when the cell is operated at 45°C. This is explained on the basis of a large ohmic drop associated with a resistive SEI, which decreases when the temperature is set to 45°C. In order to avoid any influence of the film formed at the lithium counter electrode in half cells, which is very resistive in the presence of SA, the Gr/electrolyte interface was studied by means of symmetrical Gr/Gr cells at 45°C. Cycling experiments confirm that at the first cycle the full Gr capacity is recovered when SA is not added to the electrolyte. In such symmetric cell, the reversible capacity fades upon cycling for an unknown reason but in any case, capacity values remain lower in presence of SA. This proves that SA has globally a negative impact on the Gr/electrolyte interface as well as the Li/electrolyte. XPS measurements show that the composition of the SEI formed on Gr is richer in organic and polymeric compounds and poorer in Li_nF_m clusters or lithiated species when SA is added, their scarce presence hindering lithium conduction through the SEI film. GC-MS analysis show that, after cycling in presence of SA, the electrolyte does not contain any ethylene glycol bis-(alkylcarbonate) derivatives which are commonly observed in standard alkylcarbonate based electrolytes and attributed to solvents reduction. A mechanism enlightening the role of SA during SEI formation is proposed.

Acknowledgments

The research leading to these results has received partial funding from the European Union Seventh Framework Program (FP7/2007-2013) in the framework of the Hi-C project under grant agreement no 608575.

References

1. X. Rui, Q. Yan, M. Skyllas-Kazacos, and T. M. Lim, *Journal of Power Sources*, **258**, 19 (2014).
2. Q. D. Truong, M. K. Devaraju, Y. Ganbe, T. Tomai, and I. Honma, *Electrochimica Acta*, **127**, 245 (2014).
3. J. Demeaux, D. Lemordant, M. Caillon-Caravanier, H. Galiano, and B. Claude-Montigny, *Electrochimica Acta*, **89**, 163 (2013).
4. K. Xu, *Chemical Reviews*, **104** (10), 4303 (2004).
5. H. Lee, S. Choi, S. Choi, H.-J. Kim, Y. Choi, S. Yoon, and J. -J. Cho, *Electrochemistry Communications*, **9**(4), 801 (2007).
6. V. Tarnopolskiy, J. Kalhoff, M. Nádherná, D. Bresser, L. Picard, F. Fabre, M. Rey, and S. Passerini, *Journal of Power Sources*, **236**, 39 (2013).
7. C. H. Chen, J. Liu, and K. Amine, *Journal of Power Sources*, **96**(2), 321 (2001).
8. R. Petibon, C. P. Aiken, N. N. Sinha, J. C. Burns, H. Ye, C. M. VanElzen, G. Jain, S. Trussler, and J. R. Dahn, *Journal of The Electrochemical Society*, **160**(1), A117 (2013).
9. I. J. Gordon, S. Genies, G. Si Larbi, A. Boulineau, L. Daniel, and M. Alias, *Journal of Power Sources*, **307**, 788 (2016).
10. P. Verma, P. Maire, and P. Novák, *Electrochimica Acta*, **55**(22), 6332 (2010).
11. J. G. Thevenin and R. H. Muller, *Journal of The Electrochemical Society*, **134**(2), 273 (1987).
12. M. E. Orazem and B. Tribollet, in *Electrochemical Impedance Spectroscopy*, p. 233, Wiley & Sons Ed., Hoboken, New Jersey (USA), (2008).
13. A. Lewandowski, A. Swiderska-Mocek, and L. Waliszewski, *Journal of Solid State Electrochemistry*, **16**(10), 3391 (2012).
14. R. Bouchet, S. Lascaud, and M. Rosso, *Journal of The Electrochemical Society*, **150**(10), A1385 (2003).

15. J. Rösch and R. Mülhaupt, *Polymer Bulletin*, **31**(6), 679 (1993).
16. G.-B. Han, J.-N. Lee, D. J. Lee, H. Lee, J. Song, H. Lee, M.-H. Ryou, J.-K. Park, and Y. M. Lee, *Electrochimica Acta*, **115**, 525 (2014).
17. Y. Okuno, K. Ushirogata, K. Sodeyama, and Y. Tateyama, *Physical Chemistry Chemical Physics*, **18**(12), 8643 (2016).
18. H. Hijazi, H. Rothard, P. Boduch, I. Alzaher, F. Ropars, A. Cassimi, J. M. Ramillon, T. Been, B. B. d'Etat, H. Lebius, L. S. Farenzena, and E. F. da Silveira, *Nuclear Instruments and Methods in Physics Research Section B: Beam Interactions with Materials and Atoms*, **269**(9), 1003 (2011).
19. V. Eshkenazi, E. Peled, L. Burstein, and D. Golodnitsky, *Solid State Ionics*, **170**(1–), 83 (2004).
20. D. Ensling, M. Stjerndahl, A. Nyten, T. Gustafsson, and J. O. Thomas, *Journal of Materials Chemistry*, **19**(1), 82 (2009).
21. R. I. R. Blyth, H. Buqa, F. P. Netzer, M. G. Ramsey, J. O. Besenhard, P. Golob, and M. Winter, *Applied Surface Science*, **167**, (1), 99 (2000).
22. N.-S. Choi, K. H. Yew, H. Kim, S.-S. Kim, and W.-U. Choi, *Journal of Power Sources*, **172**(1), 404 (2007).
23. S.-H. Lee, I.-S. Jo, and J. Kim, *Surface and Interface Analysis*, **46**(8), 570 (2014).
24. L. Castro, R. Dedryvère, J.-B. Ledeuil, J. Bréger, C. Tessier, and D. Gonbeau, *Journal of The Electrochemical Society*, **159**(4), A357 (2012).
25. V. Kraft, W. Weber, B. Streipert, R. Wagner, C. Schultz, M. Winter, and S. Nowak, *RSC Advances*, **6**(1), 8 (2016).
26. J.-w. Liu, X.-h. Li, Z.-x. Wang, H.-j. Guo, and Q.-y. Hu, *Chemical Research in Chinese Universities*, **25**(6), 791 (2009).
27. K. Kim, I. Park, S.-Y. Ha, Y. Kim, M.-H. Woo, M.-H. Jeong, W. C. Shin, M. Ue, S. Y. Hong, and N.-S. Choi, *Electrochimica Acta*, **225**, 358 (2017).
28. H. Kim, S. Grugeon, G. Gachot, M. Armand, L. Sannier, and S. Laruelle, *Electrochimica Acta*, **136**, 157 (2014).
29. G. Gachot, S. Grugeon, M. Armand, S. Pilard, P. Guenot, J.-M. Tarascon, and S. Laruelle, *Journal of Power Sources*, **178**(1), 409 (2008).
30. H. Kim, S. Grugeon, G. Gachot, M. Armand, L. Sannier, and S. Laruelle, *Electrochimica Acta*, **136**, 157 (2014).
31. T. Sasaki, T. Abe, Y. Iriyama, M. Inaba, and Z. Ogumi, *Journal of Power Sources*, **150**, 208 (2005).
32. G. Gachot, P. Ribière, D. Mathiron, S. Grugeon, M. Armand, J.-B. Leriche, S. Pilard, and S. Laruelle, *Analytical Chemistry*, **83**(2), 478 (2011).
33. P. J. Corish and W. H. T. Davison, *Journal of the Chemical Society*, 927 (1958).
34. D. A. Long, *Journal of Raman Spectroscopy*, **35**(10), 905 (2004).
35. S. Matsuta, T. Asada, and K. Kitaura, *Journal of The Electrochemical Society*, **147**(5), 1695 (2000).
36. P. Mirone and P. Chiorboli, *Spectrochimica Acta*, **18**(11), 1425 (1962).
37. L. L. Shevchenko, *Russian Chemical Reviews*, **32**(4), 201 (1963).
38. B. C. Smith, in *Infrared Spectral Interpretation: A Systematic Approach*, Taylor & Francis Ed., Boca Raton, Florida (USA) (1998).
39. W. A. Layman, *PhD Thesis* (1963), Montana State University, Bozeman (USA).